Received: 22 December 2020 | Revised: 18 May 2021 | Accepted: 24 May 2021

DOI: 10.1002/zamm.202000375

ORIGINAL PAPER

Triple stratification effects on bioconvective stagnation point flow pertaining carbon nanotubes due to induced magnetic field

Sujesh Areekara[1] | **Alappat Sunny Sabu**[1] | **Rakesh Kumar**[2] | **Alphonsa Mathew**[1]

[1] Department of Mathematics, St. Thomas' College (Autonomous), Thrissur 680001, India

[2] Srinivasa Ramanujan Department of Mathematics, Central University of Himachal Pradesh, Dharamshala 176215, India

Correspondence
Alphonsa Mathew, Department of Mathematics, St. Thomas' College (Autonomous), Thrissur 680001, India.
Email: alphonsa@stthomas.ac.in

The bioconvective stagnation point flow involving carbon nanotubes along a lengthening sheet subject to induced magnetic field and multiple stratification effects has been considered for investigation. Relevant similarity formulas are effectuated in converting the modelled equations into a first-order system of ODEs and are further treated in MATLAB using *ODE45* and Newton Raphson method. Illustrations on the consequence of effectual parameters on the physical quantities and the flow profiles are achieved with the aid of graphs. It is observed that the nanofluid temperature profile ascends with augmenting volume fraction and Eckert number. The numerical veracity of the present study is displayed through a restrictive study with prior published works and a commendable agreement is noted. Nusselt number is found to elevate with volume fraction and lower with thermal stratification parameter. Moreover, the findings of the present numerical exploration have applications in biomedical imaging, hyperthermia, targeted drug delivery, and cancer therapy.

KEYWORDS
carbon nanotubes, induced magnetic field, microorganisms, multiple stratification, stagnation point flow

1 | INTRODUCTION

Mass and heat transfer parades a decisive role in many aspects of engineering and medical field. The penultimate aim of scientists has been finding ways to enhance these transfer capabilities. The introduction of nanofluid (combination of fluid with nanoparticles) in place of conventional fluids by Choi [1] marked a breakthrough in the field of fluid dynamics. Buongiorno [2] promoted a two-phase nanofluid model including the seven slip mechanisms among which only Brownian motion and thermophoresis contributed in enhancing the heat transfer of nanomaterial. However, the Buongiorno model excludes the augmentation in the effective thermophysical properties of nanomaterial. Later, Tiwari and Das [3] developed a simpler nanofluid model considering the effective thermophysical properties of a nanofluid. Kumar et al. [4] utilized the Tiwari-Das nanofluid model to investigate the influence of vibrational rotations and multiple slip conditions on the hydromagnetic nanomaterial flow over an elongating surface. They observed a rise in the Nusselt number for augmenting nanoparticle volume fraction. An analytical approach to study the significance of the Hall current and Soret effect on the nanoliquid flow through an inclined channel utilizing the Tiwari-Das model was carried out

by Sabu et al. [5]. A few recent studies on the nanomaterial flow through heterogeneous configurations can be seen in [6–10].

CNT (carbon nanotube) is a graphene sheet rolled up into a tube having a nanoscale diameter. CNTs are categorised into SWCNT (single-wall carbon nanotubes) and MWCNT (multi-wall carbon nanotubes) based on the number of used graphene sheets. CNT finds its use in structural reinforcement, automotive parts, device modelling, energy storage, electromagnetic shields, etc. CNTs are also proved to be useful in the medical field. CNTs are administered in drug delivery, cancer diagnosis and treatment, thermal ablation, delivery of genetic material, etc. The significance of nonlinear thermal radiation and quartic chemical reactions on CNT-water nanomaterial flow over a lengthening surface has been explored by Kumar et al. [11]. A higher Nusselt number is noted for SWCNTs than MWCNTs. In addition, the heat transfer growth subject to different CNTs and induced magnetic field (IMF) has been examined by Raza et al. [12]. Nadeem et al. [13] conducted a numerical study to reveal that water-based SWCNT-MWCNT hybrid nanoliquid has a better heat transfer rate when balanced against SWCNT-water nanoliquid. Sreedevi and Reddy [14] performed a comparative study on the effect of water-based SWCNTs and MWCNTs Maxwell nanoliquid flow between two stretchable rotating disks. Some important analyses concerning CNTs are given in [15–17]. In this work, SWCNTs are preferred over MWCNTs due to the amelioration it provides in the medical field and also due to their lower toxicity level.

Nanofluid involving microorganisms is an advancing field that has intrigued researchers due to its relevance in antibiotics, biofuel, toxin removal, targeted drug delivery and food digestion. Bioconvection refers to the upward and downward movement of microorganisms caused by the unstable density stratification of microorganisms at the upper surface. Changes in heat, mass and motile density profiles or the presence of different fluids trigger a formation of layers known as stratification. Alsaedi et al. [18] elucidated the stratification effects of MHD mixed convective nanofluid flow past an elongated surface using HAM and observed a decrease in temperature with augmenting thermal stratification parameter. Muhammad et al. [19] scrutinized the influence of slip on the bioconvective Carreau nanoliquid flow and observed a decrease in the density of the motile microorganism with augmenting bioconvection Lewis number. A numerical exploration on the impact of swimming gyrotactic microorganisms for hydromagnetic nanofluid through a stretched porous sheet using the Darcy-Forchheimer model was carried out by Shahid et al. [20]. Various articles exploring bioconvective flows, microorganisms, and stratification effects are discussed in [21–24].

The magnetic field represents an important characteristic of hydromagnetic problems. Howbeit, studies incorporating IMF (the additional magnetic field that gets induced on electrically conducting fluid when encountered with an external magnetic field caused due to the impact of a larger magnetic Reynolds number) effects are limited in number. The induced magnetic field (IMF) has applications in MRI, glass manufacturing, geophysics, and MHD generators, etc. Kumari et al. [25] explored the fluid flow and heat transfer over an elongating sheet heeding IMF. Later, the MHD flow over a lengthening sheet subject to an IMF was reinvestigated by Ali et al. [26]. Investigations on entropy generation and IMF effects on Cu and TiO_2 nanofluid using Keller box method are carried out by Iqbal et al. [27] and observed an improved thermal conductivity for water-based TiO_2 nanofluid when compared with water based Cu nanofluid.

The stagnation point corresponds to the point where the fluid's local velocity is zero. Kumar et al. [28] explored the stagnation flow of the Casson nanomaterial through Darcy-Forchheimer medium. They noted a drop in the velocity profile of Sakiadis flow with the Casson parameter. Mahanthesh et al. [29] statistically surveyed the impact of thermal Biot number and exponential heat source parameter on the heat transfer rate. Kumar et al. [30] employed OHAM to examine the transport of nanomaterial filled in Darcy-Forchheimer medium space. Waini et al. [31] investigated the unsteady stagnation flow of a hybrid nanomaterial on a porous rigid surface and observed an increase in the heat transfer rate with augmenting mass flux parameter.

Ali et al. [32] developed the study of Mahapatra and Gupta [33] to analyse the hydromagnetic stagnation point fluid flow over a lengthening sheet subject to an IMF. Later, Junoh et al. [34] broadened the work of Ali et al. [32] to study the hybrid nanoliquid flow characteristics. Gireesha et al. [35] utilized the Runge-Kutta-Fehlberg technique to numerically explore the significance of IMF in boundary layer stagnation point flow. Further, Ijaz et al. [36] elucidated the impact of CNTs on stagnation flow involving quartic chemical reaction and IMF. Iqbal et al. [37] conducted a numerical investigation to exploit the response of IMF on transfer quantities using MWCNT and SWCNT and noted a constructive effect for nanoparticle volume fraction on the IMF profile.

However, bioconvective stagnation point flow of CNT over a lengthening sheet considering IMF, microorganisms and stratification effects has not been a topic of study to date. This paper makes an effort in filling this gap. Additionally, chemical reaction and viscous dissipation effects are also heeded.

FIGURE 1 Figurative representation

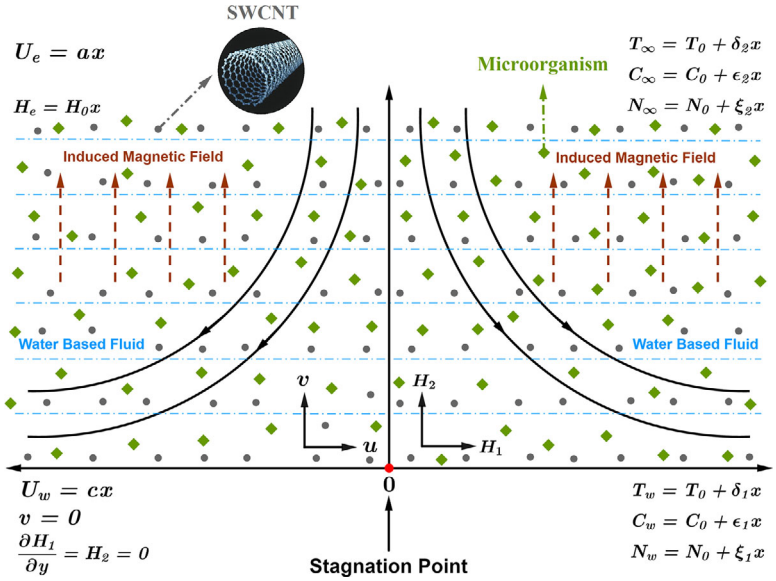

2 | MATHEMATICAL FRAME

Two-dimensional steady bioconvective stagnation point flow over a linearly elongating sheet (Figure 1) is considered under the ensuing assumptions:

(i) The expanding sheet is positioned along x axis and water-based SWCNT nanofluid containing microorganisms occupies the region $y > 0$.
(ii) $U_W(x) = cx$ and $U_e(x) = ax$ corresponds to the velocity of the lengthening sheet and the free stream, respectively.
(iii) Induced magnetic field vector, $H = (H_1, H_2)$ is considered with H_1 & H_2 being the magnetic integrants along x and y direction, respectively.
(iv) Chemical reaction and viscous dissipation effects are incorporated.
(v) Motile density, thermal, and solutal stratification effects are also considered.
(vi) The problem is modelled using the Tiwari-Das nanofluid model [3].

Following the aforementioned assumptions, the governing equations are written as (see [18, 37]):

$$\frac{\partial u}{\partial x} + \frac{\partial v}{\partial y} = 0 \tag{1}$$

$$\frac{\partial H_1}{\partial x} + \frac{\partial H_2}{\partial y} = 0 \tag{2}$$

$$u\frac{\partial u}{\partial x} + v\frac{\partial u}{\partial y} - \frac{\mu_e}{4\pi\rho_{nf}}\left(H_1\frac{\partial H_1}{\partial x} + H_2\frac{\partial H_1}{\partial y}\right) = U_e\frac{dU_e}{dx} - \frac{\mu_e H_e}{4\pi\rho_{nf}}\frac{dH_e}{dx} + \left(\frac{\mu_{nf}}{\rho_{nf}}\right)\frac{\partial^2 u}{\partial y^2} \tag{3}$$

$$u\frac{\partial H_1}{\partial x} + v\frac{\partial H_1}{\partial y} - H_1\frac{\partial u}{\partial x} - H_2\frac{\partial u}{\partial y} = \alpha_m\frac{\partial^2 H_1}{\partial y^2} \tag{4}$$

$$u\frac{\partial T}{\partial x} + v\frac{\partial T}{\partial y} = \alpha_{nf}\frac{\partial^2 T}{\partial y^2} + \frac{\mu_{nf}}{(\rho C_p)_{nf}}\left(\frac{\partial u}{\partial y}\right)^2 \tag{5}$$

$$u\frac{\partial C}{\partial x} + v\frac{\partial C}{\partial y} = D_B\frac{\partial^2 C}{\partial y^2} - k_r(C - C_\infty) \tag{6}$$

$$u\frac{\partial N}{\partial x} + v\frac{\partial N}{\partial y} + \frac{bW_c}{C_W - C_0}\left(\frac{\partial}{\partial y}\left(N\frac{\partial C}{\partial y}\right)\right) = D_m\frac{\partial^2 N}{\partial y^2} \tag{7}$$

with

$$u = U_W(x) = cx, v = 0, \frac{\partial H_1}{\partial y} = H_2 = 0, T = T_W = T_0 + \delta_1 x, C = C_W = C_0 + \epsilon_1 x, N = N_W = N_0 + \xi_1 x \quad \text{at } y = 0$$

$$u \to U_e(x) = ax, H_1 \to H_e(x) = H_0 x, T \to T_\infty = T_0 + \delta_2 x, C \to C_\infty = C_0 + \epsilon_2 x, N \to N_\infty = N_0 + \xi_2 x \quad \text{as } y \to \infty$$

where $\alpha_m = \frac{1}{4\pi\mu_e\sigma_{nf}}$ represents the magnetic diffusivity.

Introducing the following similarity transformations [18, 32, 37]:

$$u = cx f'(\zeta), v = -\sqrt{c\vartheta_f} f(\zeta), H_1 = H_0 x g'(\zeta), \zeta = y\sqrt{\frac{c}{\vartheta_f}}, H_2 = -H_0\sqrt{\frac{\vartheta_f}{c}} g(\zeta),$$

$$\theta(\zeta) = \frac{T - T_\infty}{T_W - T_0}, \psi(\zeta) = \frac{C - C_\infty}{C_W - C_0}, \chi(\zeta) = \frac{N - N_\infty}{N_W - N_0}$$

into (1) – (7), we get:

$$f''' - A_1 A_2 \left\{ (f')^2 - f f'' - \frac{\beta}{A_2} \left\{ (g')^2 - g g'' - 1 \right\} - A^2 \right\} = 0 \tag{8}$$

$$g''' - \frac{A_5}{\lambda} \{ g f'' - f g'' \} = 0 \tag{9}$$

$$\theta'' + \frac{A_3 Pr}{A_4} f \theta' + \frac{Ec\, Pr}{A_1 A_4} (f'')^2 = 0 \tag{10}$$

$$\psi'' + Le\, f \psi' - Kr\, Le\, \psi = 0 \tag{11}$$

$$\chi'' + Lb\, f \chi' - Pe \{ (\chi + \Omega) \psi'' + \chi' \psi' \} = 0 \tag{12}$$

subject to the boundary conditions

$$f(\zeta) = 0, \quad f'(\zeta) = 1, \quad g(\zeta) = 0, \quad g''(\zeta) = 0, \quad \theta(\zeta) = 1 - s_1, \quad \psi(\zeta) = 1 - s_2, \quad \chi(\zeta) = 1 - s_3 \quad \text{when } \xi = 0$$

$$f'(\zeta) \to A, \quad g'(\zeta) \to 1, \quad \theta(\zeta) \to 0, \quad \psi(\zeta) \to 0, \quad \chi(\zeta) \to 0 \quad \text{as } \xi \to \infty$$

where the dimensionless parameters are:

$$A = \frac{a}{c}, \quad \beta = \frac{\mu_e}{4\pi\rho_f}\left(\frac{H_0}{c}\right)^2, \quad \lambda = \frac{1}{4\pi\mu_e\sigma_f\vartheta_f}, \quad Pr = \frac{(\mu C_p)_f}{\kappa_f} = \frac{\vartheta_f}{\alpha_f}, \quad Kr = \frac{k_r}{c}, \quad Ec = \frac{(cx)^2}{(C_p)_f (T_W - T_0)},$$

$$Le = \frac{\vartheta_f}{D_B}, \quad Lb = \frac{\vartheta_f}{D_m}, \quad Pe = \frac{bW_c}{D_m}, \quad \Omega = \frac{N_\infty}{N_W - N_0}, \quad s_1 = \frac{\delta_2}{\delta_1}, \quad s_2 = \frac{\epsilon_2}{\epsilon_1}, \quad s_3 = \frac{\xi_2}{\xi_1}.$$

The nanofluid models incorporated are [14, 37]:

$$\text{Effective Dynamic Viscosity: } \frac{\mu_{nf}}{\mu_f} = \frac{1}{(1-\phi)^{2.5}} = \frac{1}{A_1}$$

$$\text{Effective Density: } \frac{\rho_{nf}}{\rho_f} = (1-\phi) + \phi\left(\frac{\rho_{SWCNT}}{\rho_f}\right) = A_2$$

$$\text{Effective Specific Heat: } \frac{(\rho C_p)_{nf}}{(\rho Cp)_f} = (1-\phi) + \phi\left(\frac{(\rho Cp)_{SWCNT}}{(\rho Cp)_f}\right) = A_3$$

$$\text{Effective Thermal Conductivity}: \frac{\kappa_{nf}}{\kappa_f} = \frac{(1-\phi) + 2\phi \frac{\kappa_{SWCNT}}{\kappa_{SWCNT}-\kappa_f} ln\left(\frac{\kappa_{SWCNT}+\kappa_f}{2\kappa_f}\right)}{(1-\phi) + 2\phi \frac{\kappa_f}{\kappa_{SWCNT}-\kappa_f} ln\left(\frac{\kappa_{SWCNT}+\kappa_f}{2\kappa_f}\right)} = A_4$$

$$\text{Effective Electrical Conductivity}: \frac{\sigma_{nf}}{\sigma_f} = 1 + \frac{3\left(\frac{\sigma_{SWCNT}}{\sigma_f} - 1\right)\phi}{\left(\frac{\sigma_{SWCNT}}{\sigma_f} + 2\right) - \left(\frac{\sigma_{SWCNT}}{\sigma_f} - 1\right)\phi} = A_5$$

Physical quantities in the non-dimensional form are given by [14, 18, 37]:

$$\text{Local drag coefficient}: Cf_x = \frac{\tau_\omega}{\rho_f (U_W)^2} = \frac{\mu_{nf} \frac{\partial u}{\partial y}|_{y=0}}{\rho_f (U_W)^2} \Rightarrow Cf_x \, Re_x^{1/2} = \frac{f''(0)}{A_1}$$

$$\text{Local Nusselt number}: Nu_x = \frac{x\, q_\omega}{\kappa_f (T_W - T_0)} = \frac{-x\, \kappa_{nf} \frac{\partial T}{\partial y}|_{y=0}}{\kappa_f (T_W - T_0)} \Rightarrow Nu_x \, Re_x^{-1/2} = -A_4\, \theta'(0)$$

$$\text{Local Sherwood number}: Sh_x = \frac{x\, q_m}{D_B (C_W - C_0)} = \frac{-x\, D_B \frac{\partial C}{\partial y}|_{y=0}}{D_B (C_W - C_0)} \Rightarrow Sh_x \, Re_x^{-1/2} = -\psi'(0)$$

$$\text{Local microorganism density number}: Nn_x = \frac{x\, q_n}{D_m (N_W - N_0)} = \frac{-x\, D_m \frac{\partial N}{\partial y}|_{y=0}}{D_m (N_W - N_0)} \Rightarrow Nn_x \, Re_x^{-1/2} = -\chi'(0)$$

where $Re_x = \frac{U_W\, x}{\vartheta_f}$ is the local Reynold's number.

3 | NUMERICAL SCHEME AND VALIDATION

Equations (8)– (12) together with the boundary conditions are numerically resolved in MATLAB employing *ODE45* (for solving) and Newton Raphson method (for shooting). This is accomplished by initially assuming:

$$\Gamma_1 = f, \quad \Gamma_2 = f', \quad \Gamma_3 = f'', \quad \Gamma_3{}' = f''', \quad \Gamma_4 = g, \quad \Gamma_5 = g', \quad \Gamma_6 = g'', \quad \Gamma_6{}' = g''',$$
$$\Gamma_7 = \theta, \quad \Gamma_8 = \theta', \quad \Gamma_8{}' = \theta'', \quad \Gamma_9 = \psi, \quad \Gamma_{10} = \psi', \quad \Gamma_{10}{}' = \psi'', \quad \Gamma_{11} = \chi, \quad \Gamma_{12} = \chi', \quad \Gamma_{12}{}' = \chi''$$

The reduced system of the first-order ODE is given by:

$$\Gamma_1' = \Gamma_2$$
$$\Gamma_2' = \Gamma_3$$
$$\Gamma_3' = A_1 A_2 \{ (\Gamma_2)^2 - \Gamma_1 \Gamma_3 - \frac{\beta}{A_2} \{(\Gamma_5)^2 - \Gamma_4 \Gamma_6 - 1\} - A^2 \}$$
$$\Gamma_4' = \Gamma_5$$
$$\Gamma_5' = \Gamma_6$$
$$\Gamma_6' = \frac{A_5}{\lambda} \{ \Gamma_4 \Gamma_3 - \Gamma_1 \Gamma_6 \}$$
$$\Gamma_7' = \Gamma_8$$

TABLE 1 Comparison of drag coefficient ($Cf_x Re_x^{1/2}$) for different A values between the present study and the works of Iqbal et al. [37] and Hayat et al. [38, 39] when $\phi = \beta = 0$

	$Cf_x Re_x^{1/2}$			
A	**Iqbal et al. [37]**	**Hayat et al. [38]**	**Hayat et al. [39]**	**Present study**
0.1	−0.969386	−0.96939	−0.96937	−0.9693860
0.2	−0.918107	−0.91811	−0.91813	−0.9181071
0.5	−0.667263	−0.66726	−0.66723	−0.6672637
0.7	−0.433475	−0.43346	−0.43345	−0.4334755
0.8	−0.299388	−0.29929	−0.29921	−0.2993888
0.9	−0.154716	−0.15458	−0.1545471	−0.1547167
1	0	0	0	0

TABLE 2 Comparison of $Nu_x Re_x^{-1/2}$ and $-Cf_x Re_x^{1/2}$ for differing ϕ, β, λ values between the present study and Iqbal et al. [37]

			$-Cf_x Re_x^{1/2}$		$Nu_x Re_x^{-1/2}$	
ϕ	β	λ	**Iqbal et al. [37]**	**Present study**	**Iqbal et al. [37]**	**Present study**
0.1	0	1	0.8201	0.82011	2.9371	2.93709
0.2	0	1	1.0139	1.01386	3.7139	3.71387
0	0	1	0.6673	0.66726	1.8581	1.85807
0	0.1	1	0.5759	0.57595	1.8771	1.8771
0	0.2	5	0.5129	0.51293	1.8909	1.89091
0	0.2	10	0.5651	0.56507	1.8802	1.88018

$$\Gamma_8' = -\left\{ \frac{A_3\, Pr}{A_4}\, \Gamma_1\, \Gamma_8 + \frac{Ec\, Pr}{A_1\, A_4}\, (\Gamma_3)^2 \right\}$$

$$\Gamma_9' = \Gamma_{10}$$

$$\Gamma_{10}' = Kr\, Le\, \Gamma_9 - Le\, \Gamma_1\, \Gamma_{10}$$

$$\Gamma_{11}' = \Gamma_{12}$$

$$\Gamma_{12}' = Pe\, \{ (\Gamma_{11} + \Omega)\, \Gamma_{10}' + \Gamma_{12}\, \Gamma_{10} \} - Lb\, \Gamma_1\, \Gamma_{12}$$

with

$$\Gamma_1(0) = 0, \quad \Gamma_2(0) = 1, \quad \Gamma_3(0) = \Lambda_1, \quad \Gamma_4(0) = 0, \quad \Gamma_5(0) = \Lambda_2, \quad \Gamma_6(0) = 0,$$

$$\Gamma_7(0) = 1 - s_1, \quad \Gamma_8(0) = \Lambda_3, \quad \Gamma_9(0) = 1 - s_2, \quad \Gamma_{10}(0) = \Lambda_4, \quad \Gamma_{11}(0) = 1 - s_3, \quad \Gamma_{12}(0) = \Lambda_5$$

where Λ_1 , Λ_2 , Λ_3 , Λ_4 & Λ_5 are estimated by employing the Newton Raphson method with a befitting initial guess.

The above set of equations are then numerically resolved utilizing *ODE45*, a built-in MATLAB function, with an absolute error tolerance of 10^{-6}. *ODE45* employs a fourth-order Runge-Kutta method with a self-adaptive step size for effective computation. The veracity of the code and the validation of this research work have been adjudged through a restrictive comparison of the present work with prior published works of [37–39] (showcased in Tables 1 and 2).

4 | RESULTS AND DISCUSSION

The consequence of influential parameters on microbial concentration ($\chi(\zeta)$), velocity ($f'(\zeta)$), concentration ($\psi(\zeta)$), temperature ($\theta(\zeta)$) and induced magnetic field ($g'(\zeta)$) profiles are illustrated via Figures 2-15. Changes in the aforementioned profiles due to stretching parameter (A) are graphed in Figures 2 ,4 ,7 ,11 & 14. It is perceived that augmenting A values produces a constructive effect on $f'(\zeta)$ and destructive effect on $g'(\zeta)$, $\theta(\zeta)$, $\psi(\zeta)$ & $\chi(\zeta)$.

FIGURE 2 $f'(\zeta)$ for differing A values

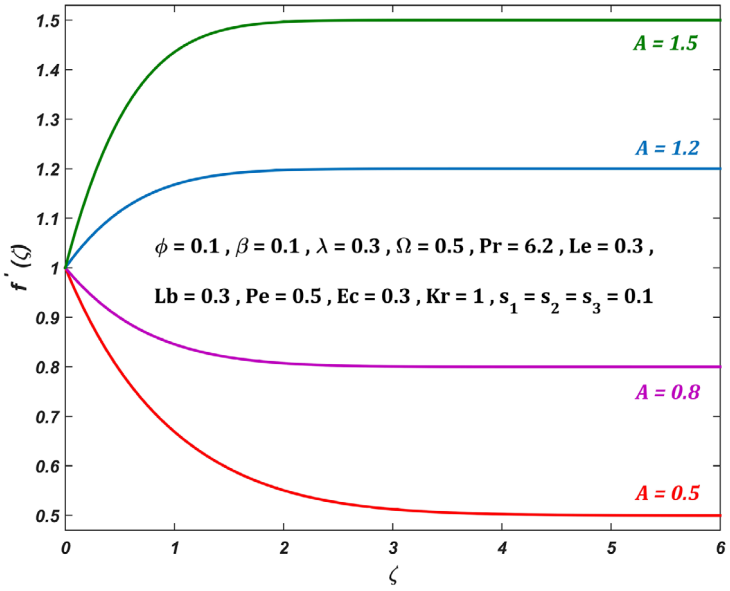

FIGURE 3 $f'(\zeta)$ for differing β values

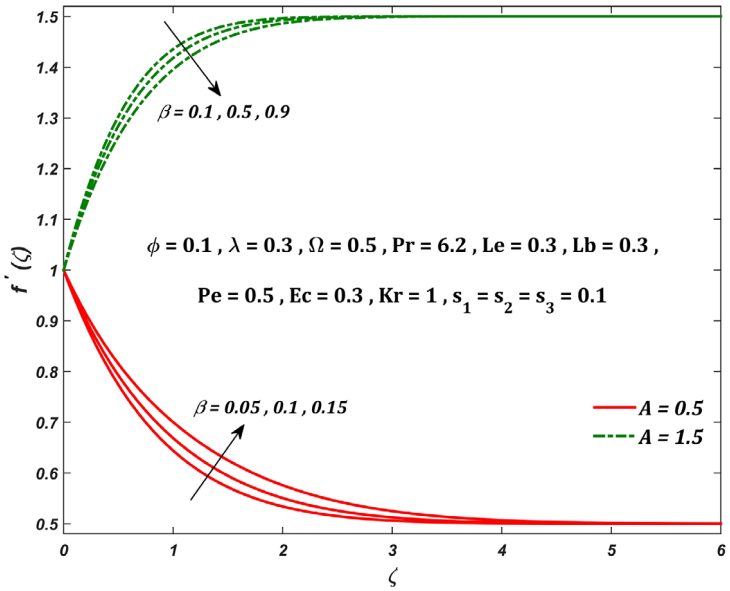

FIGURE 4 $g'(\zeta)$ for differing A values

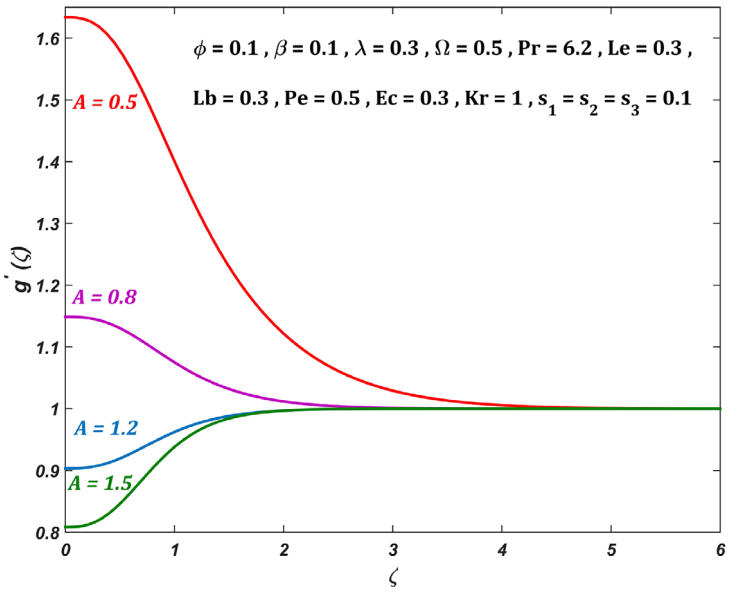

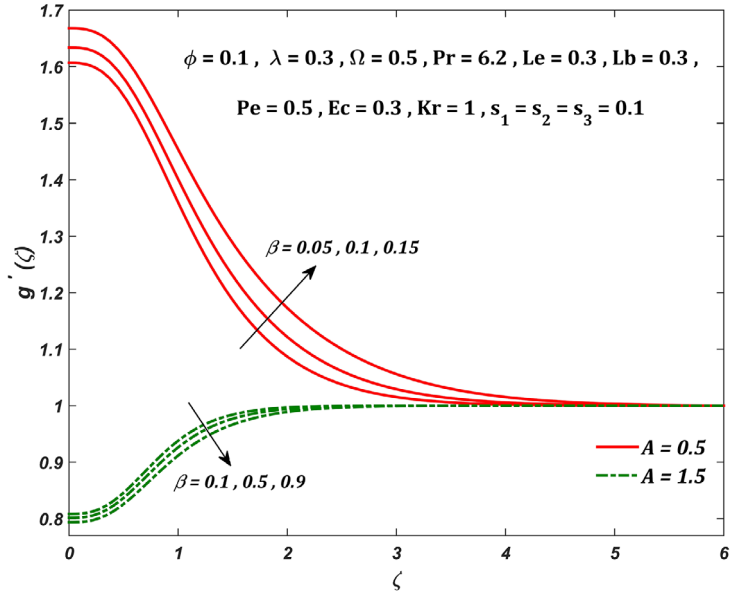

FIGURE 5 $g'(\zeta)$ for differing β values

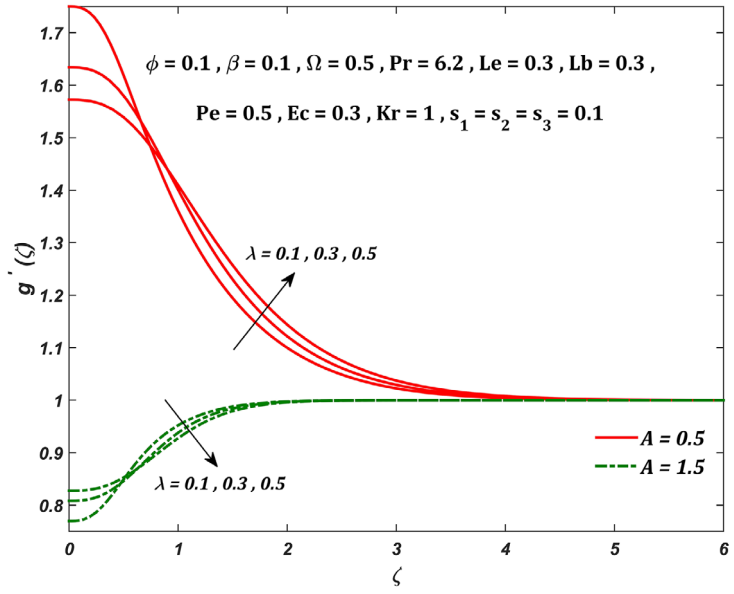

FIGURE 6 $g'(\zeta)$ for differing λ values

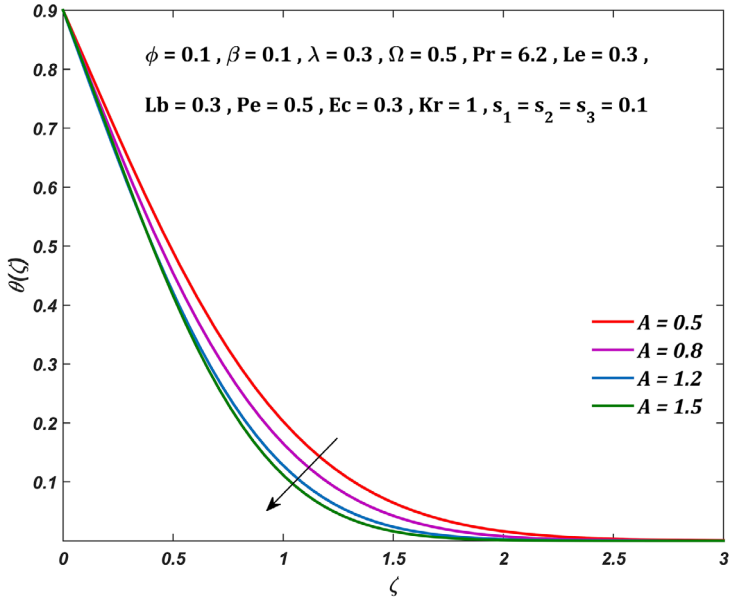

FIGURE 7 $\theta(\zeta)$ for differing A values

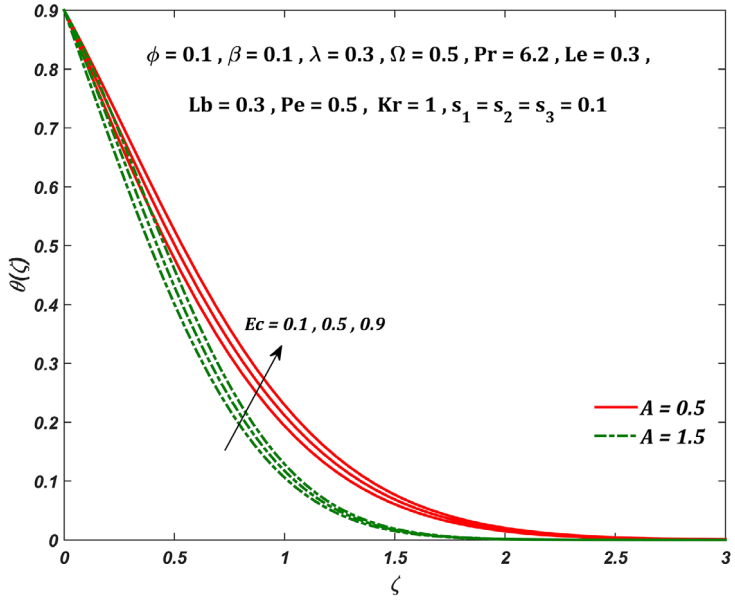

FIGURE 8 $\theta(\zeta)$ for differing Ec values

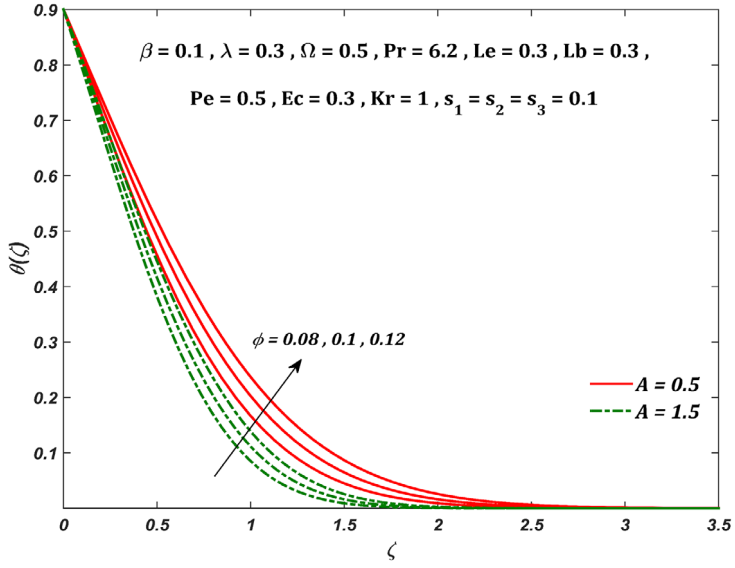

FIGURE 9 $\theta(\zeta)$ for differing ϕ values

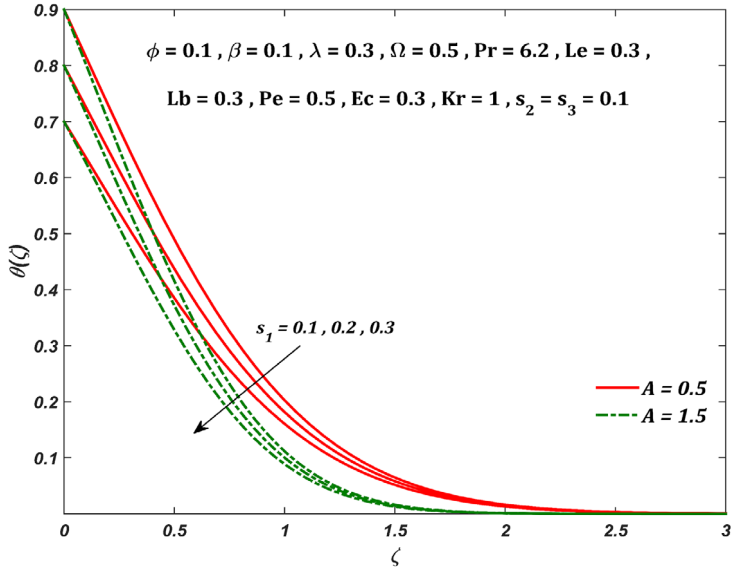

FIGURE 10 $\theta(\zeta)$ for differing s_1 values

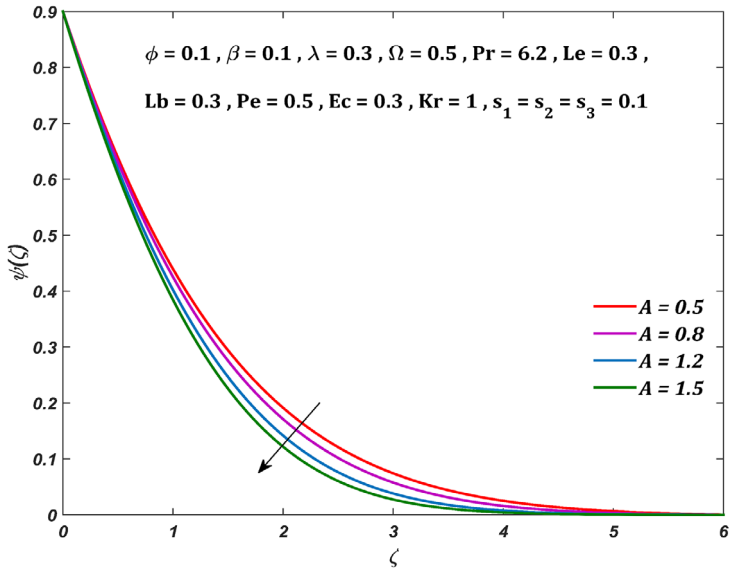

FIGURE 11 $\psi(\zeta)$ for differing A values

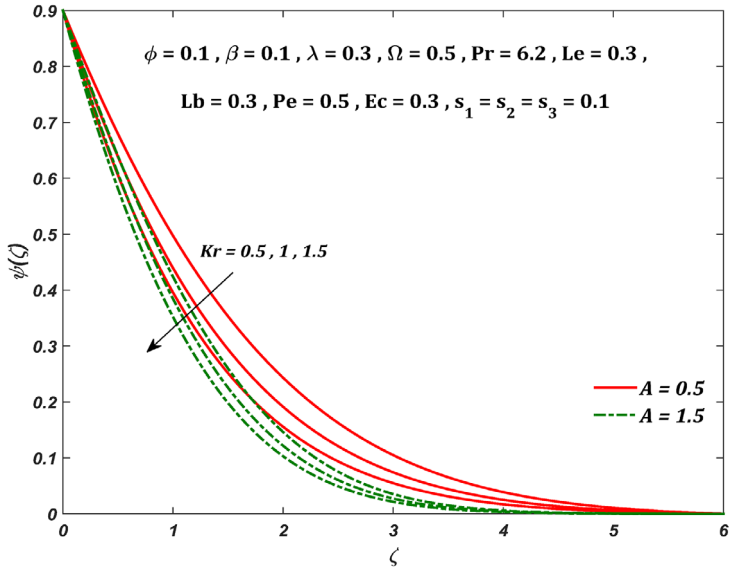

FIGURE 12 $\psi(\zeta)$ for differing Kr values

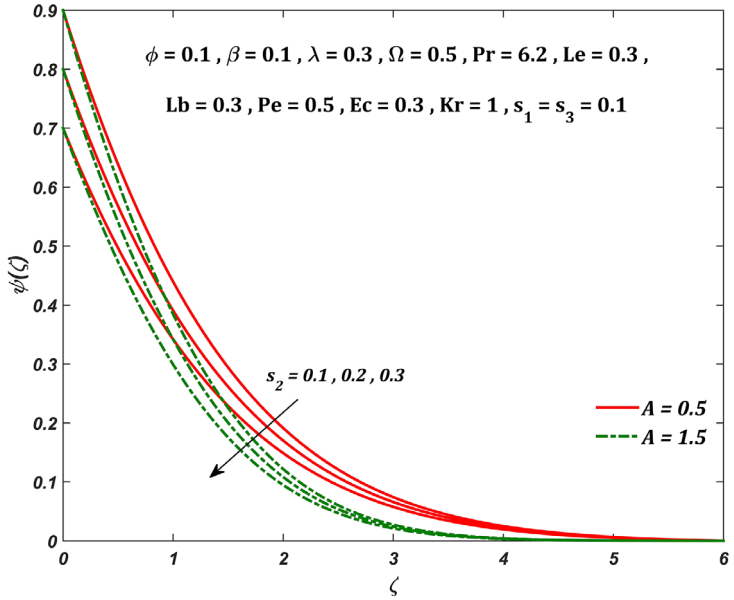

FIGURE 13 $\psi(\zeta)$ for differing s_2 values

FIGURE 14 $\chi(\zeta)$ for differing A values

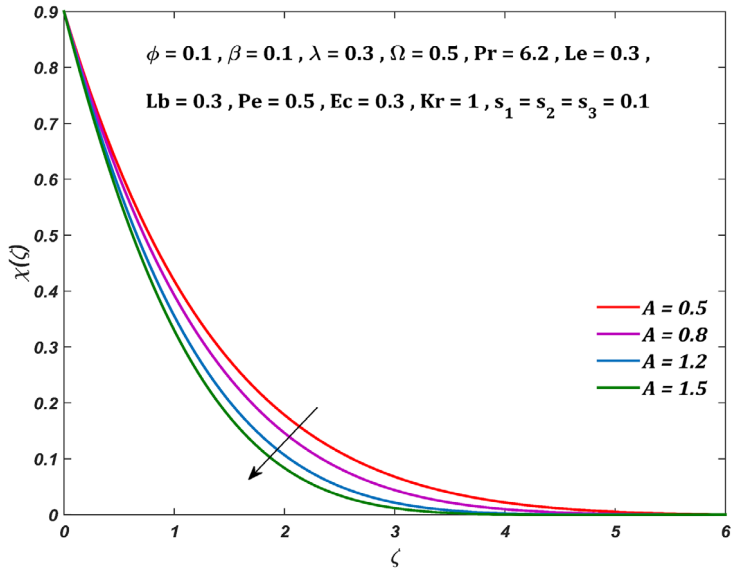

FIGURE 15 $\chi(\zeta)$ for differing s_3 values

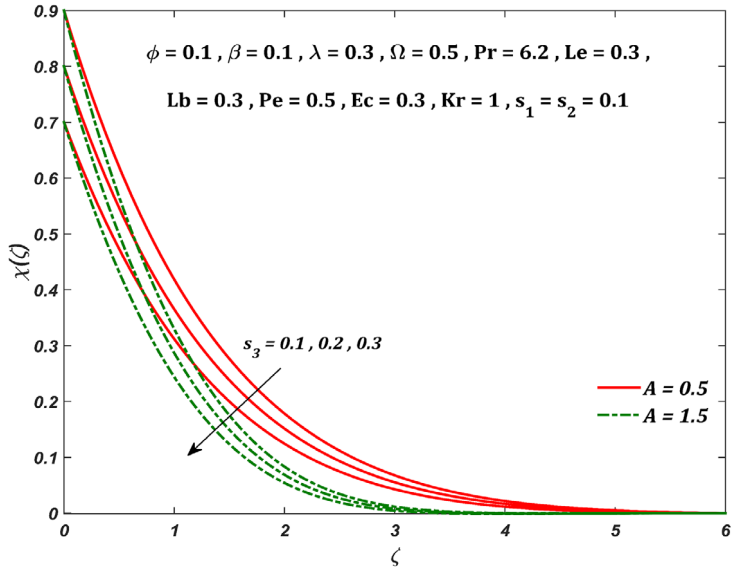

Simultaneous effects of parameters on physical quantities are depicted in Figures 16–20. Studies have been carried out for $A = 0.5$ & $A = 1.5$ with Prandtl number(Pr) and infinity fixed at 6.2 and 6, respectively. Thermophysical properties of the conventional fluid (water) and SWCNT (nanofluid) are showcased in Table 3.

Figure 3 bespeaks the deviations in $f'(\zeta)$ with respect to β (magnetic parameter). It is noted that $f'(\zeta)$ increases for augmenting β values when $A = 0.5$ and a reversed behaviour is observed for $f'(\zeta)$ when $A = 1.5$. Figure 5 depicts the influence of β on $g'(\zeta)$. An elevation in $g'(\zeta)$ for $A = 0.5$ and a demotion when $A = 1.5$ is observed for elevating β values. Figure 6 explains the mixed effect of λ (reciprocal of magnetic Prandtl number) on $g'(\zeta)$. Initially, elevating λ values

TABLE 3 Thermophysical properties of water and SWCNT (see [14, 37])

Property	Water (base fluid)	SWCNT (nanoparticle)
ρ	997	2600
C_p	4179	425
κ	0.613	6600
σ	0.05	10^6

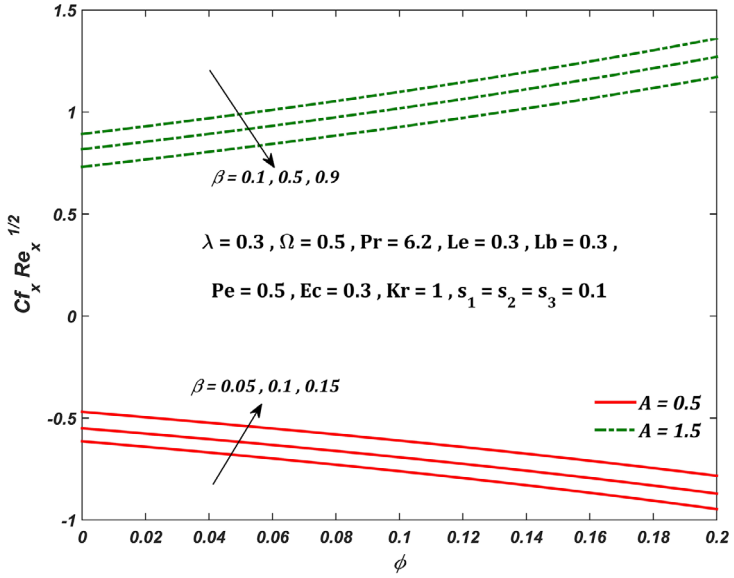

FIGURE 16 Parallel effect of ϕ & β on $Cf_x Re_x^{1/2}$

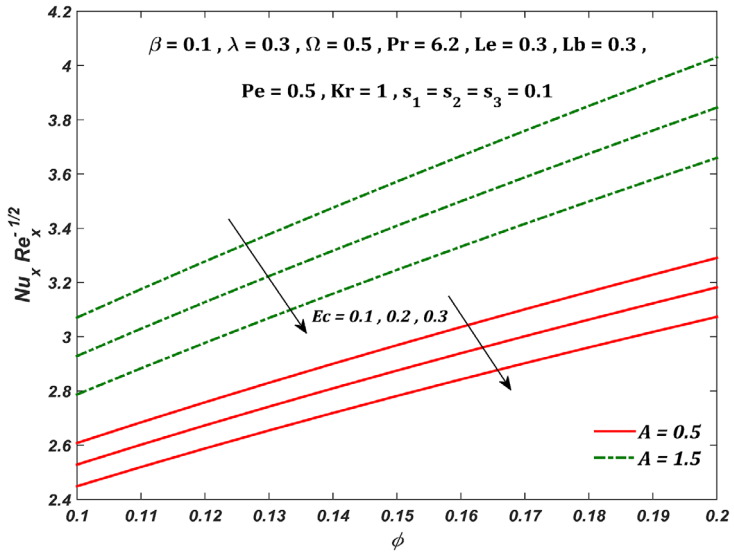

FIGURE 17 Parallel effect of ϕ & Ec on $Nu_x Re_x^{-1/2}$

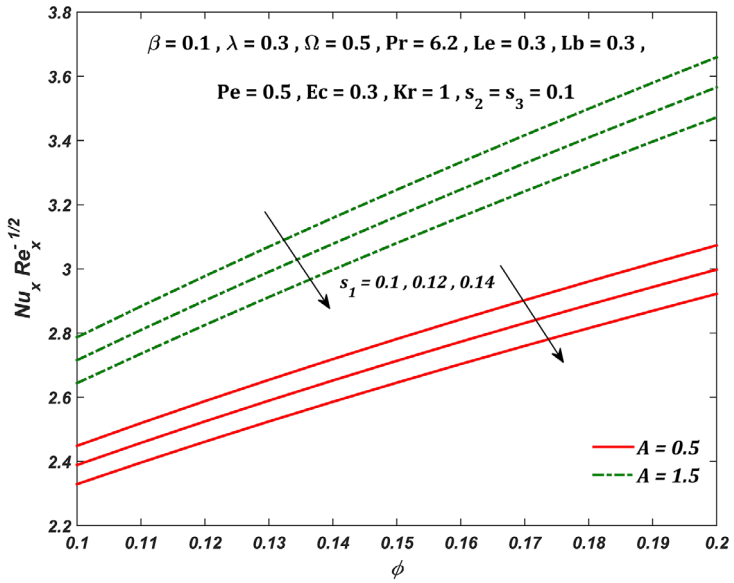

FIGURE 18 Parallel effect of ϕ & s_1 on $Nu_x Re_x^{-1/2}$

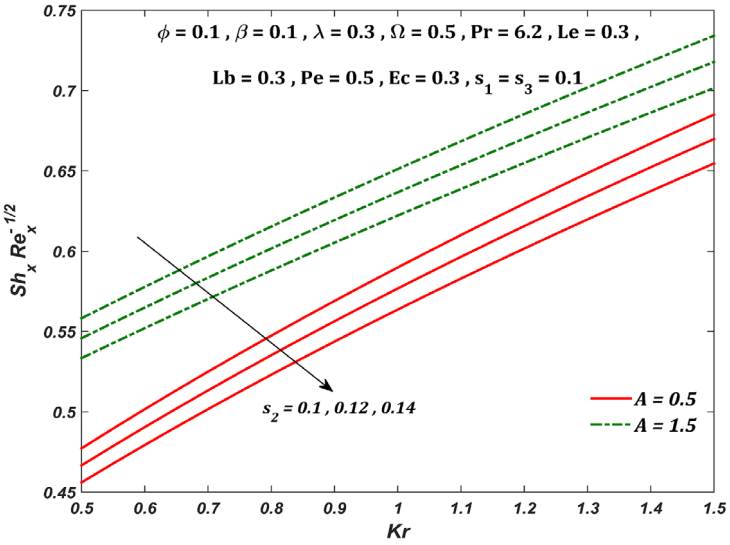

FIGURE 19 Parallel effect of Kr & s_2 on $Sh_x Re_x^{-1/2}$

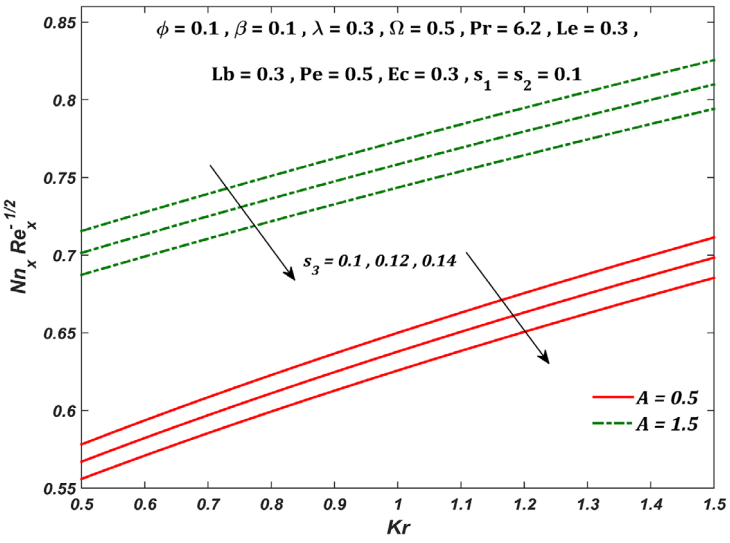

FIGURE 20 Parallel effect of Kr & s_3 on $Nn_x Re_x^{-1/2}$

decays $g'(\zeta)$ and afterwards, a reversed trend is observed when $A = 0.5$. A similar but inversed impact is perceived when $A = 1.5$.

Variation in $\theta(\zeta)$ due to Eckert number (Ec) is elucidated in Figure 8 and it is noted that augmenting Ec numerals fuels an increase in $\theta(\zeta)$. Physically, this result can be associated with the generation of friction forces between the fluid particles which increases the nanomaterial temperature.. The ascending nature of $\theta(\zeta)$ with ϕ (volume fraction of nanoparticle) is illustrated in Figure 9. This increase in temperature can be physically related to the improvement in the thermal conductivity of the nanoliquid caused by larger nanoparticle occupancy. Figure 10 explains the consequence of s_1 (thermal stratification parameter) on $\theta(\zeta)$. A decreasing behaviour is noticed and this is due to the waning temperature differences. Physically, the decrease in the nanofluid temperature is due to the drop in the temperature difference between the surface and away from the surface caused by an increase in s_1.

With a rise in the magnitude of Kr (chemical reaction parameter), depletion in $\psi(\zeta)$ is observed which has been plotted in Figure 12. The physical explanation being that the increased chemical reaction eats up the nanoparticle which induces shrinkage in the concentration profile. Figure 13 reveals the change in $\psi(\zeta)$ with ascending s_2 (solutal stratification parameter). An increase in s_2 prompts a decrease in the volumetric fraction which sources a fall in $\psi(\zeta)$. Physically, an increase in s_2 descends the concentration profile due to the decrease in the volumetric fraction between the surface and reference nanoparticles. Figure 15 describes the negative influence of s_3 (motile density stratification parameter) on $\chi(\zeta)$. This is because an augmentation in s_3 decreases the concentration difference of microorganisms between the surface and away from the surface and hence the microbial concentration decreases.

One can interpret from Figure 16 that $Cf_x Re_x^{1/2}$ increases with β and decreases with ϕ when $A = 0.5$. For $A = 1.5$, $Cf_x Re_x^{1/2}$ improves with ϕ and deteriorates with β . From Figures 17 & 18, it is clear that $Nu_x Re_x^{-1/2}$ (both cases) ascends with ϕ and descends with Ec & s_1. Figure 19 demonstrates the escalating and declining behaviour of Kr & s_2 on $Sh_x Re_x^{-1/2}$ (both cases), respectively. Figure 20 depicts that Kr causes a rise in $Nn_x Re_x^{-1/2}$ (both cases) whereas a fall in $Nn_x Re_x^{-1/2}$ (both cases) is observed due to s_3.

5 | CONCLUSION

The key points noted from the study are:

- The nanomaterial velocity is directly proportional to the magnetic parameter for $A = 0.5$ and inversely proportional when $A = 1.5$.
- Drag coefficient (when $A = 0.5$) ascends with magnetic parameter and descends with nanoparticle volume fraction. However, the results are reversed when $A = 1.5$.
- Eckert number and nanoparticle volume fraction exhibit a constructive effect on the temperature profile.
- Heat transfer is elevated due to nanoparticle volume fraction and lowered with Eckert number and thermal stratification parameter.
- Chemical reaction parameter has a destructive effect on concentration profile.
- Chemical reaction parameter promotes and solutal stratification demotes mass transfer.
- A decline in microorganism, concentration and temperature profiles is observed due to ascending motile density, solutal, thermal stratification parameters, respectively.
- Microorganism density number lowers with motile density stratification parameter.

ORCID

Sujesh Areekara https://orcid.org/0000-0001-7860-8268
Alappat Sunny Sabu https://orcid.org/0000-0002-3294-7130
Alphonsa Mathew https://orcid.org/0000-0002-3810-4484

REFERENCES

[1] Choi, S.U.S., Eastman, J.A.: Enhancing thermal conductivity of fluids with nanoparticles. Proceedings of the 1995 International Mechanical Engineering Congress and Exposition, ASME, San Francisco 66, 99–105 (1995)
[2] Buongiorno, J.: Convective transport in nanofluids. J. Heat Transfer. 128(3), 240–250 (2005)
[3] Tiwari, R.K., Das, M.K.: Heat transfer augmentation in a two-sided lid-driven differentially heated square cavity utilizing nanofluids. Int. J. Heat Mass Transf. 50, 2002–2018 (2007)
[4] Kumar, R., Kumar, R., Ali Shehzad, S., Sheikholeslami, M.: Rotating frame analysis of radiating and reacting ferro-nanofluid considering Joule heating and viscous dissipation. Int. J. Heat Mass Transf. 120, 540–551 (2018)
[5] Sabu, A.S., Mathew, A., Neethu, T.S., George, K.A.: Statistical analysis of MHD convective ferro-nanofluid flow through an inclined channel with hall current, heat source and Soret effect. Therm. Sci. Eng. Prog. 22, 100816 (2021)
[6] Kumar, R., Sharma, T., Kumar, R., Sheikholeslami, M., Vajravelu, K.: Stability analysis of multiple solutions in case of a stretched nanofluid flow obeying Corcione's correlation: an extended Darcy model. Z. Angew. Math. Mech. 101(5), e202000172 (2020)
[7] Chu, Y.M., Kumar, R., Bach, Q.: Water-based nanofluid flow with various shapes of Al2O3 nanoparticles owing to MHD inside a permeable tank with heat transfer. Appl. Nanosci. (2020) https://doi.org/10.1007/s13204-020-01609-2
[8] Aly, A.M.: Natural convection of Al2O3-water nanofluid filled annulus between a wavy rectangle and a square cavity using Buongiorno's two-phase model. Z. Angew. Math. Mech. 100(9), e202000002 (2020)
[9] Neethu, T.S., Areekara, S., Mathew, A.: Statistical approach on 3D hydromagnetic flow of water-based nanofluid between two vertical porous plates moving in opposite directions. Heat Transfer (2021) https://doi.org/10.1002/htj.22120
[10] Job, V.M., Gunakala, S.R.: Numerical study on mixed convective flow of water-based magnetite nanofluid through a wavy channel containing porous blocks under the effect of an oscillating magnetic field. Z. Angew. Math. Mech. e202000254 (2021)
[11] Kumar, R., Kumar, R., Sheikholeslami, M., Chamkha, A.J.: Irreversibility analysis of the three dimensional flow of carbon nanotubes due to nonlinear thermal radiation and quartic chemical reactions. J. Mol. Liq. 274, 379-392 (2019)
[12] Raza, M., Ellahi, R., Sait, S.M., Sarafraz, M.M., Shadloo, M.S., Waheed, I.: Enhancement of heat transfer in peristaltic flow in a permeable channel under induced magnetic field using different CNTs. J. Therm. Anal. Calorim. 140(3), 1277-1291 (2020)
[13] Nadeem, S., Hayat, T., Khan, A.U.: Numerical study on 3D rotating hybrid SWCNT-MWCNT flow over a convectively heated stretching surface with heat generation/absorption. Phys. Scr. 94(7), 075202 (2019)

[14] Sreedevi, P., Sudarsana Reddy, P.: Effect of SWCNTs and MWCNTs Maxwell MHD nanofluid flow between two stretchable rotating disks under convective boundary conditions. Heat Transfer-Asian Res. 48(8), 4105–4132 (2019)
[15] Sreedevi, P., Sudarsana Reddy, P.: Heat and mass transfer analysis of MWCNT–kerosene nanofluid flow over a wedge with thermal radiation. Heat Transfer 50(1), 10-33 (2021)
[16] Gholinia, M., Hosseinzadeh, K., Ganji, D.D.: Investigation of different base fluids suspend by CNTs hybrid nanoparticle over a vertical circular cylinder with sinusoidal radius. Case Stud. Therm. Eng. 21, 100666 (2020)
[17] Reddy, P.S., Sreedevi, P.: Effect of thermal radiation and volume fraction on carbon nanotubes based nanofluid flow inside a square chamber. Alexandria Eng. J. 60(1), 1807-1817 (2021)
[18] Alsaedi, A., Khan, M.I., Farooq, M., Gull, N., Hayat, T.: Magnetohydrodynamic (MHD) stratified bioconvective flow of nanofluid due to gyrotactic microorganisms. Adv. Powder Technol. 28(1), 288–298 (2017)
[19] Muhammad, T., Alamri, S.Z., Waqas, H., Habib, D., Ellahi, R.: Bioconvection flow of magnetized Carreau nanofluid under the influence of slip over a wedge with motile microorganisms. J. Therm. Anal. Calorim. 143(2), 945–957 (2021)
[20] Shahid, A., Huang, H., Bhatti, M.M., Zhang, L., Ellahi, R.: Numerical investigation on the swimming of gyrotactic microorganisms in nanofluids through porous medium over a stretched surface. Mathematics 8(3), 380 (2020)
[21] Md Basir, M.F., Kumar, R., Md Ismail, A.I., Sarojamma, G., Narayana, P.V.S., Raza, J., Mahmood, A.: Exploration of thermal-diffusion and diffusion-thermal effects on the motion of temperature-dependent viscous fluid conveying microorganism. Arab. J. Sci. Eng. 44(9), 8023–8033 (2019)
[22] Tlili, I., Ramzan, M., Nisa, H.U., Shutaywi, M., Shah, Z., Kumam, P.: Onset of gyrotactic microorganisms in MHD micropolar nanofluid flow with partial slip and double stratification. J. King Saud Univ. - Sci. 32(6), 2741–2751 (2020)
[23] Naz, R., Tariq, S., Sohail, M., Shah, Z.: Investigation of entropy generation in stratified MHD Carreau nanofluid with gyrotactic microorganisms under Von Neumann similarity transformations. Eur. Phys. J. Plus. 135(2), 178 (2020)
[24] Bhatti, M.M., Shahid, A., Abbas, T., Alamri, S.Z., Ellahi, R.: Study of activation energy on the movement of gyrotactic microorganism in a magnetized nanofluids past a porous plate. Processes 8(3), 328 (2020)
[25] Kumari, M., Takhar, H.S., Nath, G.: MHD flow and heat transfer over a stretching surface with prescribed wall temperature or heat flux. Wärme - und Stoffübertragung 25(6), 331–336 (1990)
[26] Ali, F.M., Nazar, R., Arifin, N.M., Pop, I.: MHD boundary layer flow and heat transfer over a stretching sheet with induced magnetic field. Heat Mass Transfer 47(2), 155–162 (2011)
[27] Iqbal, Z., Maraj, E.N., Azhar, E., Mehmood, Z.: Framing the performance of induced magnetic field and entropy generation on Cu and TiO2 nanoparticles by using Keller box scheme. Adv. Powder Technol. 28(9), 2332–2345 (2017)
[28] Kumar, R., Kumar, R., Vajravelu, K., Sheikholeslami, M.: Three dimensional stagnation flow of Casson nanofluid through Darcy-Forchheimer space: a reduction to Blasius/Sakiadis flow. Chinese J. Phys. 68, 874–885 (2020)
[29] Mahanthesh, B., Mackolil, J., Shehzad, S.A.: Statistical analysis of stagnation - point heat flow in Williamson fluid with viscous dissipation and exponential heat source effects. Heat Transfer 49(8), 4580–4591 (2020)
[30] Kumar, R., Kumar, R., Sharma, T., Sheikholeslami, M.: Mathematical modeling of stagnation region nanofluid flow through Darcy – Forchheimer space taking into account inconsistent heat source/sink. J. Appl. Math. Comput. 65, 713-734 (2021)
[31] Waini, I., Ishak, A., Pop, I.: Unsteady hybrid nanofluid flow on a stagnation point of a permeable rigid surface. Z. Angew. Math. Mech. e202000193 (2020)
[32] Ali, F.M., Nazar, R., Arifin, N.M., Pop, I.: MHD stagnation-point flow and heat transfer towards stretching sheet with induced magnetic field. Appl. Math. Mech. - Engl. Ed. 32, 409–418 (2011)
[33] Mahapatra, T.R., Gupta, A.S.: Heat transfer in stagnation-point flow towards a stretching sheet. Heat Mass Transfer 38(6), 517–521 (2002)
[34] Junoh, M.M., Ali, F.M., Arifin, N.M., Bachok, N., Pop, I.: MHD stagnation-point flow and heat transfer past a stretching/shrinking sheet in a hybrid nanofluid with induced magnetic field. Int. J. Numer. Methods Heat Fluid Flow. 30(3), 1345–1364 (2020)
[35] Gireesha, B.J., Mahanthesh, B., Shivakumara, I.S., Eshwarappa, K.M.: Melting heat transfer in boundary layer stagnation-point flow of nanofluid toward a stretching sheet with induced magnetic field. Eng. Sci. Technol. Int. J. 19(1), 313–321 (2016)
[36] Khan, M.I., Hayat, T., Shah, F., Mujeeb-Ur-Rahman, Haq, F.,: Physical aspects of CNTs and induced magnetic flux in stagnation point flow with quartic chemical reaction. Int. J. Heat Mass Transf. 135, 561–568 (2019)
[37] Iqbal, Z., Azhar, E., Maraj, E.N.: Transport phenomena of carbon nanotubes and bioconvection nanoparticles on stagnation point flow in presence of induced magnetic field. Phys. E Low-Dimensional Syst. Nanostruct. 91, 128–135 (2017)
[38] Hayat, T., Farooq, M., Alsaedi, A.: Homogeneous-heterogeneous reactions in the stagnation point flow of carbon nanotubes with Newtonian heating. AIP Adv. 5(2), 027130 (2015)
[39] Hayat, T., Muhammad, K., Farooq, M., Alsaedi, A.: Melting heat transfer in stagnation point flow of carbon nanotubes towards variable thickness surface. AIP Adv. 6(1), 015214 (2016)

How to cite this article: S. Areekara, AS. Sabu, R. Kumar, A. Mathew. Triple stratification effects on bioconvective stagnation point flow pertaining carbon nanotubes due to induced magnetic field. *Z Angew Math Mech*. 2021;e202000375. https://doi.org/10.1002/zamm.202000375